ICE SHEETS

Pervasive ice sheet mass loss reflects competing ocean and atmosphere processes

Ben Smith[1]*, Helen A. Fricker[2], Alex S. Gardner[3], Brooke Medley[4], Johan Nilsson[3], Fernando S. Paolo[3], Nicholas Holschuh[5,6], Susheel Adusumilli[2], Kelly Brunt[7], Bea Csatho[8], Kaitlin Harbeck[9], Thorsten Markus[4], Thomas Neumann[4], Matthew R. Siegfried[10], H. Jay Zwally[4,7]

Quantifying changes in Earth's ice sheets and identifying the climate drivers are central to improving sea level projections. We provide unified estimates of grounded and floating ice mass change from 2003 to 2019 using NASA's Ice, Cloud and land Elevation Satellite (ICESat) and ICESat-2 satellite laser altimetry. Our data reveal patterns likely linked to competing climate processes: Ice loss from coastal Greenland (increased surface melt), Antarctic ice shelves (increased ocean melting), and Greenland and Antarctic outlet glaciers (dynamic response to ocean melting) was partially compensated by mass gains over ice sheet interiors (increased snow accumulation). Losses outpaced gains, with grounded-ice loss from Greenland (200 billion tonnes per year) and Antarctica (118 billion tonnes per year) contributing 14 millimeters to sea level. Mass lost from West Antarctica's ice shelves accounted for more than 30% of that region's total.

Observations of ice sheet mass change are essential to our understanding of present and future sea level change (*1*–*3*). Ice sheets gain mass through snow accumulation and lose it through three processes: surface melt runoff (Greenland, 50 to 65%), iceberg calving (Antarctica, ~50%, and Greenland, 15 to 25%), and basal melting of floating ice shelves (Antarctica, ~50%) and tidewater glaciers (Greenland, 15 to 25%) (*4*–*6*). The net balance between these competing processes largely dictates decadal to centennial ice sheet contributions to sea level and depends on interactions between ice, ocean, and atmosphere. Surface meltwater runoff, basal melting, and precipitation are all expected to increase in a warming climate, which has been observed for both ice sheets (*7*, *8*). In Greenland, with a sea level potential of ~7 m, enhanced surface melt has resulted in widespread thinning of the ablation zone (*9*), and thinning and retreat of tidewater glacier fronts have led to accelerated flow (*10*), increased discharge toward the ocean (*6*), and near-coastal thinning (*11*–*13*) owing to increased flux divergence. In Antarctica, with a sea level potential of ~58 m, changes in ocean heat content linked to changes in Southern Hemisphere atmospheric conditions (*14*) have enhanced basal melting of ice shelves, causing them to shrink (*15*, *16*), which has reduced their buttressing capability and has led to increased ice discharge into the ocean (*17*–*20*). Despite rapid advancement in our ability to observe the ice sheet response to climate change, observation of ice mass changes associated with atmospheric and ocean forcing of the ice sheets with a self-consistent data set has been challenging. We used measurements from NASA's Ice, Cloud and land Elevation Satellite (ICESat; 2003–2009) and ICESat-2 (2018–2019) missions to resolve precise patterns of ice sheet height change, which when combined with a new firn model provide a combined estimate of total grounded and floating mass change from both ice sheets. Although loss of floating ice makes no direct contribution to sea level, it directly affects the rate of ice flow into the ocean. Patterns of change in floating and grounded ice together reveal the spatial signatures of the atmospheric and ocean processes that lead to grounded ice loss.

Satellite radar and laser altimeters have collected nearly continuous measurements since the early 1990s, providing one of the longest records of ice sheet change and revealing broad patterns of mass change across both ice sheets (*21*, *22*). In Antarctica, grounded ice changes have been qualitatively linked to floating ice shelf changes, but altimeter studies have all considered grounded ice (*1*, *23*) and floating ice (*1*, *16*) separately. The resulting differences in instruments, methodologies, and study periods can obscure connections between processes in grounded and floating ice, so a unified estimate of, for example, the ratio between grounded and floating ice loss has not been straightforward. Compared with radar altimetry, laser altimetry has the advantage of definitive measurement of the ice sheet surface with minimal subsurface penetration and the capability for accurate measurements over the steeper sloping ice sheet margins. ICESat, Earth's first polar-orbiting satellite laser altimeter, sampled the surface with small (~60 m) footprints and fine sampling (172 m), but results from that mission alone span only the short (6 years) duration of the mission. Subtle

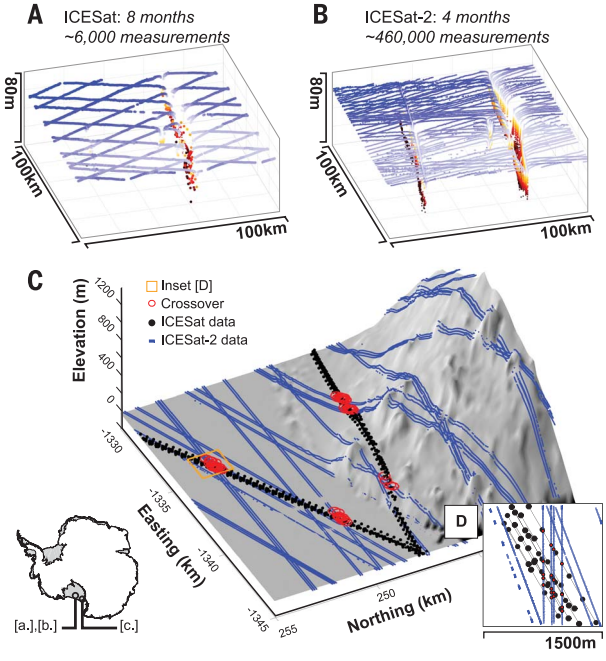

Fig. 1. Relative observation density of ICESat and ICESat-2 over the same target: Rifts of Ross Ice Shelf. (**A**) ICESat. (**B**) ICESat-2. Increased along-track resolution and cross-track observation density allow us to capture high-slope, small-scale features in unprecedented detail. (**C** and **D**) ICESat–ICESat-2 surface height comparison is done at the survey crossover points (red). ICESat-2's small footprint and dense along-track spacing [(D), to scale], combined with its repeat-track mission design, will result in the most precise measurements of height-change rates available to date.

[1]Polar Science Center, Applied Physics Laboratory, University of Washington, Seattle, WA, USA. [2]Scripps Institution of Oceanography, University of California, San Diego, La Jolla, CA, USA. [3]Jet Propulsion Laboratory, California Institute of Technology, Pasadena, CA, USA. [4]Cryospheric Science Laboratory, NASA Goddard Space Flight Center, Greenbelt, MD, USA. [5]Department of Earth and Space Sciences, University of Washington, Seattle, WA, USA. [6]Department of Geology, Amherst College, Amherst, MA, USA. [7]Earth System Science Interdisciplinary Center, University of Maryland, College Park, MD, USA. [8]Department of Geological Sciences, University at Buffalo, Buffalo, NY, USA. [9]KBR, Greenbelt, MD, USA. [10]Department of Geophysics, Colorado School of Mines, Golden, CO, USA.
*Corresponding author. Email: besmith@uw.edu

changes in the ice sheet interiors have been difficult to capture because of measurement uncertainties [time-varying biases in radar altimetry (*2*) and ICESat (*24*)]. When integrated over the vast ice sheet area, these biases can overwhelm small, but important, changes in ice sheet mass balance from either trends in precipitation or long-term imbalance between ice flow, accumulation, and runoff (*1*).

NASA's next-generation laser altimeter ICESat-2 was designed to eliminate many of these problems. Launched 15 September 2018, ICESat-2's laser has a high sampling rate (0.7 m along-track), narrow footprint (~14.5 m), and near-global coverage (±88° latitude) repeating every 3 months, with a six-beam geometry that enables instantaneous cross-track slope determination (fig. S1). We compared ICESat-2 data (October 2018 to February 2019) with data from the ICESat mission (September 2003 to October 2008), which sampled a more coarsely spaced set of tracks to ±86° latitude (Fig. 1A) (*25*). Height-change estimates from these instruments cover all of Greenland and 95% of Antarctica. We removed the influence of local topography between missions by extracting height-difference measurements only at locations where the two sets of tracks cross (Fig. 1, C and D). Because both measurements come from laser altimeters, they are not strongly biased by subsurface scattering and retain their accuracy in sloping coastal regions. After aggregating the difference measurements into a regular grid, we estimated height-change rates and applied several corrections to obtain equivalent changes in mass, including a customized firn correction, state-of-the-art glacial isostatic adjustment, elastic compensation of Earth's surface, ocean tides, and inverse barometer effect (*25*). We restricted our ice shelf analysis to areas that were covered by ice shelves throughout both missions, so the ice shelf mass changes directly associated with changes in ice shelf extent are excluded from our estimates.

In Greenland, we found strong thinning that extends around the entire coastline (Fig. 2), which decreases inland, giving way to thickening at elevations between 2000 and 2500 m in western and southern Greenland and at elevations closer to 1500 m in the northeast. The largest thinning rates were between 4 and 6 m year^{-1} in Jakobshavn and Kangerlussuaq glaciers, whereas the largest inland thickening rates were less than 0.15 m year^{-1}. The total mass change rate for the ice sheet between 2003 and 2019 was −200 ± 12 Gt year^{-1}, with a basin-by-basin variation from −48 ± 4 Gt year^{-1} in the northwest to 2 ± 2 Gt year^{-1}

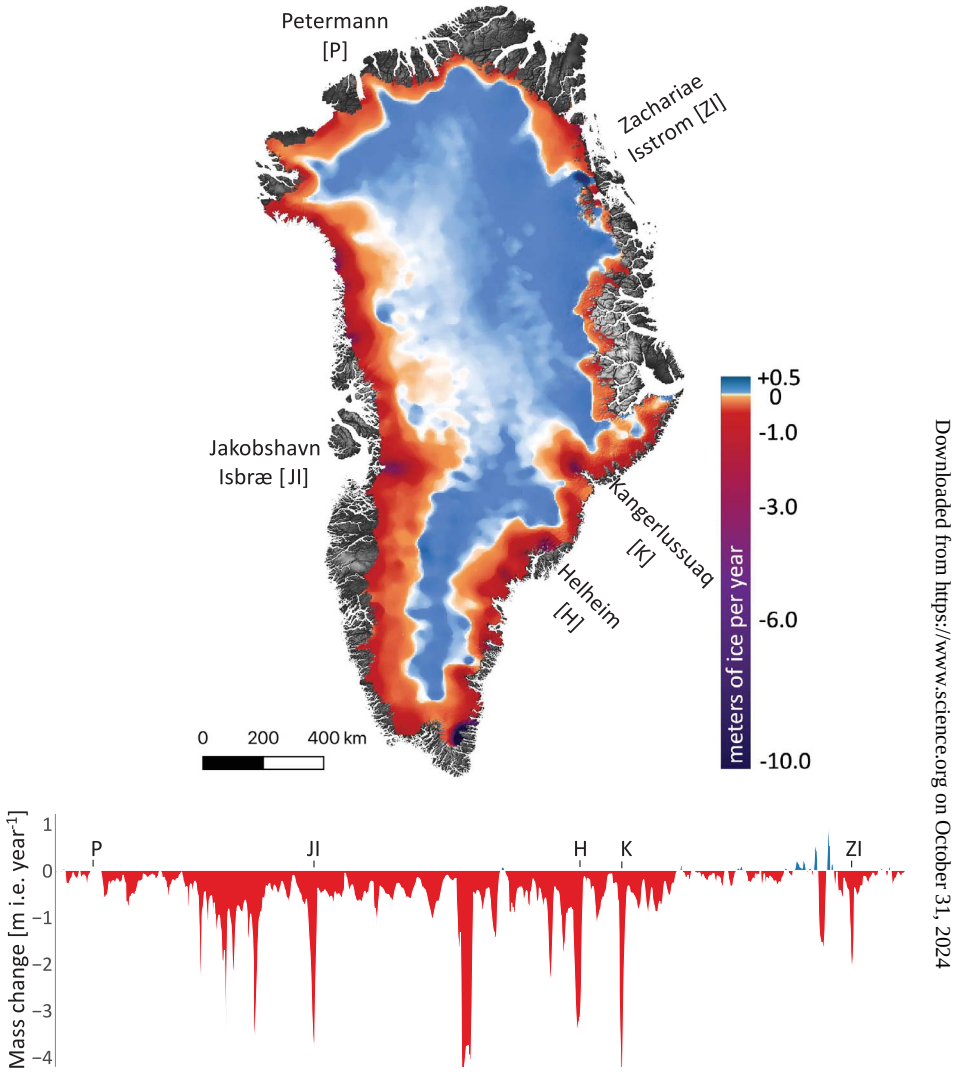

Fig. 2. Mass loss from Greenland Ice Sheet (2003 to 2019). (**Top**) Mass change for Greenland (meters of ice equivalent per year). (**Bottom**) Mass changes around the margin. Map and ice margin mass change have been smoothed with a 35-km median filter for improved visualization.

Table 1. Comparison of mass loss 2003 to 2019 for floating and grounded ice by region. SLE potential data are after (*44*): Greenland, East Antarctica (EAIS), West Antarctica (WAIS), and the Antarctic Peninsula (AP) (fig. S8). Cumulative ice loss and gain between 2003 and 2019 are provided in sea level equivalent (SLE) units.

	Change in mass over time (Gt year^{-1})		Sea level rise potential (m)	Total SLE 2003–2019 (mm)
	Floating ice	Grounded ice		
Greenland	N/A	−200 ± 12	7.4	8.9
EAIS	106 ± 29	90 ± 21	51.1	−4.0
WAIS	−76 ± 49	−169 ± 10	5.6	7.5
AP	−14 ± 28	−39 ± 5	0.5	1.7
Antarctica	15 ± 65	−118 ± 24	57.2	5.2

in the northeast (table S2). The low-elevation thinning is associated with both atmospheric and ocean processes: an increase in surface melt owing to a combination of increases in both air temperatures and exposure of bare ice during the summer (*26*–*28*). At the same time, the combination of increased surface melt and warmer ocean temperatures has led to enhanced submarine melting of submerged glacier termini (*29*, *30*) and has allowed more rapid calving by reducing the presence of rigid mélange in the fjords (*31*), each of which have increased glacier velocities and ice discharge into the ocean. With the exception of the northeast, every sector of the ice sheet lost substantial mass during our period of investigation.

Some of the highest Greenland ice mass losses are in the northwest and southeast sectors, where strong dynamic changes took place shortly after the start of the ICESat mission (*32*). The recent acceleration in ice loss from Northeast Greenland (*33*) appears more limited in extent and magnitude and has less impact on the total mass balance. Despite the record-setting discharge rates of Jakobshavn Isbrae (*34*), its contribution is only around 10% of the Greenland mass loss between 2003 and 2019, in part because the rapid mass loss due to its acceleration in the late 1990s (*35*) declined with the slowing and thickening of the lower part of the glacier between 2013 and 2018 (*36*). Overall, loss of solid ice around the margins outpaced lower rates of snow gain distributed across the interior.

In Antarctica, we see broad-scale patterns that are the fingerprints of two competing climate processes: snow accumulation and ocean melting. These processes occur on different spatial and temporal scales (Fig. 3) and exhibit strong connections between changes in grounded and floating ice in West Antarctica and the Antarctic Peninsula. The "background" pattern is one of subtle thickening along the steep slopes of the Antarctic Peninsula and around the coast to Queen Maud Land, East Antarctica, where gains decrease with distance from the ocean, which is indicative of snow accumulation in excess of that needed to balance flux divergence due to ice flow. This is likely due to enhanced moisture flux from marine air masses, but our measurements only provide an upper bound on the duration over which this may have occurred. Superimposed on this is a pattern of dramatic, ongoing mass loss around the margins, especially in the Amundsen and Bellingshausen regions of West Antarctica, which is likely in response to rapidly shrinking ice shelves. Ice shelf thinning in the Amundsen Sea has been attributed to an increase in atmospheric-driven incursions of modified Circumpolar Deep Water under the ice shelves, enhancing ocean-induced melting of marine-based basins (*14*, *16*). Similar patterns may be emerging for marine-based outlet glaciers of East Antarctica, such as at Denman Glacier (Fig. 3), where a deep subglacial canyon and a retrograde slope may drive unstable retreat (*37*). The three large cold-water ice shelves (Ross, Filchner-Ronne, and Amery) have smaller rates of height change, but there are striking internally driven changes where the stagnant Kamb Ice Stream (*38*) and slowing Whillans Ice Stream (*39*) starve downstream Ross Ice Shelf of mass input (locations are provided in fig. S8). In contrast to West Antarctic ice shelves, East Antarctic ice shelves gained 106 ± 29 Gt year^{-1} (Table 1).

The most substantial floating-ice losses occurred along the Amundsen-Bellingshausen region of West Antarctica and the Antarctic Peninsula. A basin-by-basin comparison between floating and grounded ice loss allows us to quantify the link between rapidly thinning ice shelves and grounded-ice loss in these regions; for example, 53% of mass loss from the Getz Ice Shelf basin (basin 20), 29% from

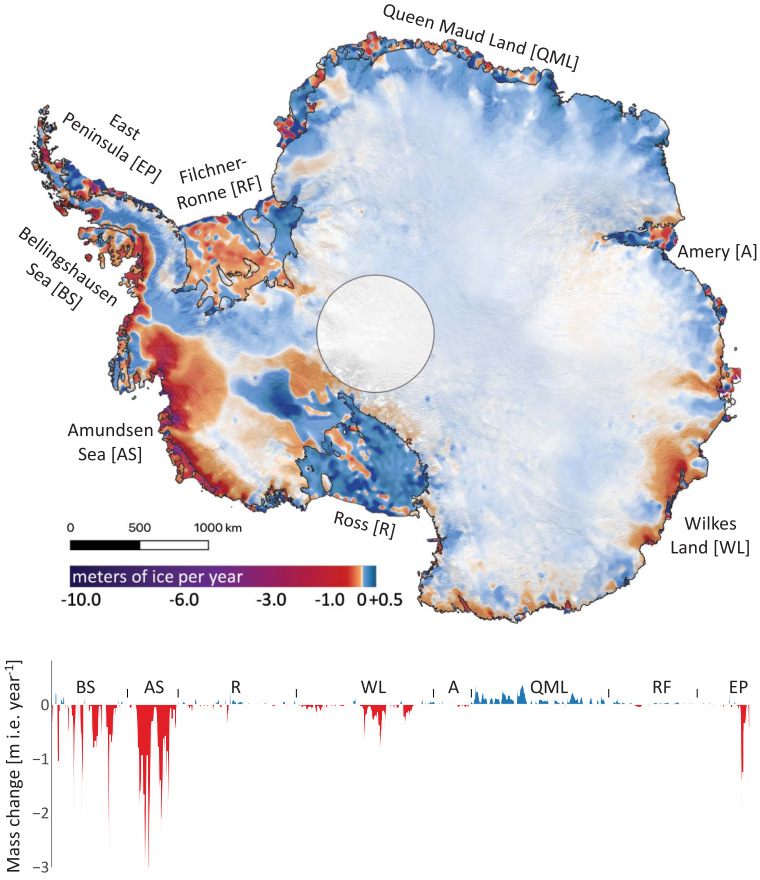

Fig. 3. Mass loss from Antarctica (2003 to 2019). (**Top**) Mass change for Antarctica. (**Bottom**) Mass changes at the grounding line. Highest mass loss rates are in West Antarctica and Wilkes Land, East Antarctica. Map and grounding line mass change have been smoothed with a 35-km median filter for improved visualization.

the Thwaites basin (basin 21), and 61% from the George VI Ice Shelf basin (basin 24) was from ice shelf mass loss. Overall, 31% of West Antarctic ice loss for 2003 to 2019 (76 ± 49 Gt year^{-1}) was from the ice shelves, whereas the remaining 69% (169 ± 10 Gt year^{-1}) was from the grounded ice feeding those ice shelves (Table 1 and table S1); for the Antarctic Peninsula, 27% of the mass loss was from floating ice.

Considering only grounded ice (for sea level contribution), our data show pervasive mass loss around the margins of Greenland, West Antarctica, and the Antarctic Peninsula, partially offset by mass gains in East Antarctica and central Greenland. Our mass loss rates of 118 ± 24 Gt year^{-1} from Antarctica and 200 ± 12 Gt year^{-1} from Greenland imply a total sea level contribution of 14 ± 1 mm over the 16-year period (Table 1). Compared with a compilation of mass-change estimates for a similar time span (2002 to 2017) (*2*), our Antarctic estimates are consistent (within reported errors) for the Antarctic Peninsula and for the whole ice sheet but significantly more positive for East Antarctica (90 ± 21 versus 2 ± 37 Gt year^{-1}) and significantly more negative for West Antarctica (–169 ± 10 versus –124 ± 27 Gt year^{-1}). For Greenland, our estimate is consistent with rates derived from a compilation of techniques that extends through 2018 (*40*) but is significantly more positive than some rates calculated from mass-flux techniques between 2003 and 2018 (–200 ± 12 versus –268 ± 14 Gt year^{-1}) (*41*). Another recent mass-flux–based estimate (*42*) gives modestly larger loss rates for Greenland (–233 + 12 Gt year^{-1}), with differences that arise in part because that estimate includes mass changes in peripheral ice and tundra that our study excludes. Because our estimates of height change have smaller instrumental biases than those of previous laser-altimetry estimates, our results suggest that earlier disagreement between some input-output and altimetry estimates (*1*, *8*) was at least partially due to negative biases in the input-output estimates. Despite this, our results show that the mass gains in East Antarctica are not sufficient to offset the rapid mass losses from West Antarctica and the Antarctic Peninsula, so that Antarctica's contribution to sea level change is unambiguously positive.

We estimated height changes for both ice sheets (grounded and floating ice) from NASA's ICESat and ICESat-2 laser altimetry missions (2003 to 2019). Applying new corrections to convert from height to mass change, we generated maps of mass changes for the ice sheets. Our maps highlight complex localized patterns of ocean-induced changes near the coast where inland ice is responding to increased frontal melt and ice shelf thinning by flowing faster, leading to increased flux divergence and surface lowering, with the strongest signals in the Amundsen and Bellingshausen coasts of Antarctica. Mixed signals, including the effects of surface melting and ocean-driven velocity changes, are apparent around the coasts of Greenland. We also see more subtle thickening across the vast interiors of the ice sheets, likely in response to increased snowfall, where the precision of measurements of height change by previous altimeters limited inferences of mass change. For both ice sheets, these patterns result from the interplay between the ocean and atmosphere; ultimately, high-elevation gains are greatly outmatched by low-elevation dynamic losses, combined with enhanced surface melting in Greenland.

Our unified estimates of grounded and floating ice sheet mass change show that overall, Greenland lost 200 ± 12 Gt year^{-1}, while Antarctica lost a total of 103 Gt year^{-1}, with 118 ± 24 Gt year^{-1} from grounded ice and a small net gain of 15 ± 65 Gt year^{-1} from ice shelves. Together, the ice sheets contributed ~14 mm sea level equivalent to the global oceans over that 16-year period (8.9 mm from Greenland and 5.2 mm from Antarctica). In West Antarctica, ice loss from ice shelves (which does not directly contribute to sea level change) accounted for 31% of the total mass loss, and all West Antarctic marine basins with ice grounded below sea level (which are sensitive to flow instabilities and whose losses directly contribute to sea level change) are out of balance. Given the susceptibility of ice shelves and floating glacier termini to changing atmospheric and oceanic conditions, and of grounded ice to shrinking ice shelves (*43*), we can expect increasing contribution from both Greenland and Antarctica to sea level rise on relatively short (decadal to centennial) time scales.

REFERENCES AND NOTES

1. A. Shepherd *et al*., *Science* **338**, 1183–1189 (2012).
2. IMBIE team, *Nature* **558**, 219–222 (2018).
3. J. L. Bamber, R. M. Westaway, B. Marzeion, B. Wouters, *Environ. Res. Lett.* **13**, 63008 (2018).
4. D. I. Benn, T. Cowton, J. Todd, A. Luckman, *Curr. Clim. Change Rep.* **3**, 282–290 (2017).
5. M. A. Depoorter *et al*., *Nature* **502**, 89–92 (2013).
6. E. Rignot, S. Jacobs, J. Mouginot, B. Scheuchl, *Science* **341**, 266–270 (2013).
7. J. T. M. Lenaerts, B. Medley, M. R. van den Broeke, B. Wouters, *Rev. Geophys.* **57**, 376–420 (2019).
8. E. Rignot *et al*., *Proc. Natl. Acad. Sci. U.S.A.* **116**, 1095–1103 (2019).
9. M. van den Broeke *et al*., *Science* **326**, 984–986 (2009).
10. I. Joughin *et al*., *J. Geophys. Res. Earth Surf* **117**, F02030 (2012).
11. B. M. Csatho *et al*., *Proc. Natl. Acad. Sci. U.S.A.* **111**, 18478–18483 (2014).
12. I. M. Howat, B. E. Smith, I. Joughin, T. A. Scambos, *Geophys. Res. Lett.* **35**, L17505 (2008).
13. N. Wilson, F. Straneo, P. Heimbach, *Cryosphere* **11**, 2773–2782 (2017).
14. M. Thoma, A. Jenkins, D. Holland, S. Jacobs, *Geophys. Res. Lett.* **35**, L18602 (2008).
15. H. D. Pritchard *et al*., *Nature* **484**, 502–505 (2012).
16. F. S. Paolo, H. A. Fricker, L. Padman, *Science* **348**, 327–331 (2015).
17. J. J. Fürst *et al*., *Nat. Clim. Chang.* **6**, 479–482 (2016).
18. T. K. Dupont, R. B. B. Alley, *Geophys. Res. Lett.* **32**, 1–4 (2005).
19. T. A. Scambos, J. A. Bohlander, C. A. Shuman, P. Skvarca, *Geophys. Res. Lett.* **31**, L18402 (2004).
20. E. Rignot, J. Mouginot, M. Morlighem, H. Seroussi, B. Scheuchl, *Geophys. Res. Lett.* **41**, 3502–3509 (2014).
21. D. J. Wingham, A. Shepherd, A. Muir, G. J. Marshall, *Philos. Trans. A Math. Phys. Eng. Sci.* **364**, 1627–1635 (2006).
22. H. J. Zwally *et al*., *J. Glaciol.* **51**, 509–527 (2005).
23. H. D. Pritchard, R. J. Arthern, D. G. Vaughan, L. A. Edwards, *Nature* **461**, 971–975 (2009).
24. A. A. Borsa, H. A. Fricker, K. M. Brunt, *IEEE Trans. Geosci. Remote Sens.* **57**, 6946–6959 (2019).
25. Materials and methods are available as supplementary materials.
26. J. C. Ryan *et al*., *Nat. Commun.* **9**, 1065 (2018).
27. M. R. van den Broeke *et al*., *Cryosphere* **10**, 1933–1946 (2016).
28. X. Fettweis *et al*., *Cryosphere* **11**, 1015–1033 (2017).
29. M. Wood *et al*., *Geophys. Res. Lett.* **45**, 8334–8342 (2018).
30. D. Slater *et al*., *Cryosphere* **13**, 2489–2509 (2019).
31. T. Moon, I. Joughin, B. Smith, *J. Geophys. Res. Earth Surf.* **120**, 818–833 (2015).
32. E. Rignot, P. Kanagaratnam, *Science* **311**, 986–990 (2006).
33. S. A. Khan *et al*., *Nat. Clim. Chang.* **4**, 292–299 (2014).
34. I. Joughin, B. E. Smith, D. E. Shean, D. Floricioiu, *Cryosphere* **8**, 209–214 (2014).
35. I. Joughin, W. Abdalati, M. Fahnestock, *Nature* **432**, 608–610 (2004).
36. A. Khazendar *et al*., *Nat. Geosci.* **12**, 277–283 (2019).
37. M. Morlighem *et al*., *Nat. Geosci.* **13**, 132–137 (2020).
38. G. A. Catania, T. A. Scambos, H. Conway, C. F. Raymond, *Geophys. Res. Lett.* **33**, L14502 (2006).
39. L. H. Beem *et al*., *J. Geophys. Res. Earth Surf.* **119**, 212–224 (2014).
40. IMBIE Team, *Nature* **579**, 233–239 (2020).
41. J. Mouginot *et al*., *Proc. Natl. Acad. Sci. U.S.A.* **116**, 9239–9244 (2019).
42. M. D. King *et al*., *Cryosphere* **12**, 3813–3825 (2018).
43. G. H. Gudmundsson, F. S. Paolo, S. Adusumilli, H. A. Fricker, *Geophys. Res. Lett.* **46**, 13903–13909 (2019).
44. K. J. Tinto *et al*., *Nat. Geosci.* **12**, 441–449 (2019).

ACKNOWLEDGMENTS

We thank the ICESat-2 project and the ICESat-2 science team for enormous contributions to this project. We are also grateful to two anonymous reviewers for their constructive and insightful reviews. **Funding:** This work was funded by the NASA Cryospheric Sciences Program in support of the ICESat-2 mission under the following awards: NNX15AE15G (to B.S.); NNX15AC80G (to H.A.F.); NNX16AM01G (to N.H.); NNX17AI03G (to H.A.F.). A.S.G., J.N., and F.S.P. were funded by the NASA Cryospheric Sciences and NASA MEaSUREs programs through direct award to A.S.G. **Author contributions:** H.A.F., B.S., and A.S.G. conceptualized the study and, with F.S.P., wrote the majority of the main text. B.M. conducted firn and climate modeling. F.S.P., S.A., and J.N. performed altimetry data processing. N.H., F.S.P., J.N., and A.S.G. developed figures. K.B. provided insights into error models and calibrations. B.C., M.R.S., and H.J.Z. provided insights into altimetry and data analysis. T.N., T.M., and K.H. were responsible for the success of the ICESat-2 mission. All authors contributed to the writing and editing of the manuscript. **Competing interests:** The authors report no competing interests. **Data and materials availability:** ICESat data are available at https://nsidc.org/data/gla12, and the ICESat-2 data are available at https://nsidc.org/data/atl06. Mass-change grids are available from https://digital.lib.washington.edu/researchworks/handle/1773/45388 (accession no. 45388).

SUPPLEMENTARY MATERIALS

science.sciencemag.org/content/368/6496/1239/suppl/DC1
Materials and Methods
Supplementary Text
Figs. S1 to S8
Tables S1 and S2
References (*45–100*)

20 September 2019; accepted 13 April 2020
Published online 30 April 2020
10.1126/science.aaz5845